Effect of Gravity on Manipulation Performance of a Robotic Arm

Tasuku YAMAWAKI and Masahito YASHIMA
Dept. of Mechanical Systems Engineering
National Defense Academy of Japan
Yokosuka, Kanagawa 239-8686, JAPAN
{yamawaki, yashima}@nda.ac.jp

***Abstract*— The present paper introduces an evaluation of the manipulation performance of a robotic arm with respect to control accuracy and mechanical efficiency, taking into consideration the effects of gravity and the dynamic process between inputs and outputs in the robotic system. A measure based on the output controllability ellipsoid is proposed, which shows the relationship between the end-effector motion and the joint driving force. Computer simulations demonstrate the effects of gravity on the manipulation performance and the benefits of the proposed measure for the trajectory planning.**

I. INTRODUCTION

Robotic arms generally work in gravitational fields. Therefore, we need to evaluate the manipulation performance of the robotic arm by taking into consideration the gravitational effect. Several measures for the manipulation capabilities of a robotic arm have been proposed. These measures are useful to the design of an arm mechanism, the trajectory planning, and the determination of an optimal posture for a given task.

Qualitative measures based on the kinematic relationship between the joint angular velocity and the end-effector motion have been developed [3], [8], [12]. Yoshikawa [12] proposed the manipulability ellipsoid for measuring the ease of changing the end-effector by a set of joint velocities with fixed magnitude and showed the manipulability measure by the volume of the ellipsoid.

The arm dynamics cannot be ignored for a precise and high-speed manipulation or for a detailed mechanical design. Considering the arm dynamics, a number of performance measures have been proposed [1], [2], [5], [10], [12]. By extending the concept of manipulability to the dynamic case, Yoshikawa [12] proposed the dynamic manipulability ellipsoid based on the relationship between the end-effector acceleration and the joint driving force and showed the dynamic manipulability measure.

Here, we discuss the manipulation performance from the viewpoint of the system theory. As shown in Fig. 1, there is causality between the input and the output in the system, and the characteristics of the entire system can be evaluated from the state of its output for the given input. In the case of the dynamic manipulability, the performance of a robotic arm is evaluated based on the state of end-effector accelerations (output) for the given joint driving forces (input) at the moment. Therefore, the dynamic manipulability is regarded as the measure of the static process.

To achieve a given task, it is important that the end-effector can be arbitrary manipulated by applying the joint driving forces in a finite time. Therefore, the manipulation performance of a robotic arm should be considered from the viewpoint of a dynamic process rather than a static process. In addition, it is necessary to consider the gravitation, which affects the dynamic process in this system.

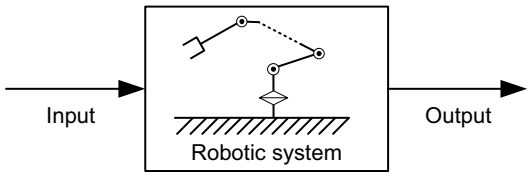

Fig. 1. Concept of dynamic process and static process in the robotic system

From the linear system theory, the output controllability of the dynamic system indicates the effect of its input on its output. Since quantitative measures of the output controllability have been proposed [4], [11], the concept of the linear system theory can be applied to the evaluation of the manipulation performance.

In the present paper, the evaluation for the manipulation performance taking gravity into consideration is proposed. We present a useful ellipsoid, which expresses the set of output controllable displacements of the end-effector in terms of the given joint torque. The volume, shape, and orientation of the ellipsoid can yield the performance evaluation of the mechanical efficiency and the control accuracy of the robotic arm quantitatively. We show the evaluation examples of the two degree-of-freedom robotic arm and the two application examples for the trajectory planning.

II. CRITERIA FOR CONTROLLABILITY

This section describes the definition of state controllability and output controllability and their basic properties. Let the state vector be $\boldsymbol{x} \in \Re^q$, the input vector be $\boldsymbol{u} \in \Re^r$, the output vector be $\boldsymbol{y} \in \Re^m$, and the time be $t > 0_-$. The state equation and the output equation of a linear time-invariant system can be described as

$$\dot{\boldsymbol{x}}(t) = \boldsymbol{A}\boldsymbol{x}(t) + \boldsymbol{B}\boldsymbol{u}(t) \tag{1}$$

$$\boldsymbol{y}(t) = \boldsymbol{C}\boldsymbol{x}(t) \tag{2}$$

$$\boldsymbol{A} \in \Re^{q\times q}, \boldsymbol{B} \in \Re^{q\times r}, \boldsymbol{C} \in \Re^{m\times q}$$

Here, we input the linear sum of an impulse function $\delta(t)$ and its derivative as $\delta^{(k)} = d\delta^{k-1}(t)/dt$. This impulsive

input can be written as

$$\boldsymbol{u}(t) = \boldsymbol{h}_1\delta(t) + \cdots + \boldsymbol{h}_q\delta^{(q-1)}(t) \tag{3}$$

where $\boldsymbol{h}_i \in \Re^m$ is weight vector for the input. Substituting $\boldsymbol{u}(t)$ into (1) and integrating it from $t = 0_-$ to $t = 0_+$ yields [7]

$$\boldsymbol{x}(0_+) - \boldsymbol{x}(0_-) = \begin{bmatrix}\boldsymbol{B} & \boldsymbol{AB} & \cdots & \boldsymbol{A}^{q-1}\boldsymbol{B}\end{bmatrix}\begin{bmatrix}\boldsymbol{h}_1 \\ \vdots \\ \boldsymbol{h}_q\end{bmatrix} \tag{4}$$

A system is said to be state controllable if any initial state $\boldsymbol{x}(0_-)$ can be transferred to any final state at $t = t_+$. The necessary and sufficient condition for state controllability is that the controllability matrix

$$\boldsymbol{V} \triangleq \begin{bmatrix}\boldsymbol{B} & \boldsymbol{AB} & \cdots & \boldsymbol{A}^{q-1}\boldsymbol{B}\end{bmatrix} \in \Re^{q\times qr} \tag{5}$$

has full rank q [7].

Equations (2) and (4) yield an equation in terms of output $\boldsymbol{y}(t)$, such as

$$\boldsymbol{y}(0_+) - \boldsymbol{y}(0_-) = \boldsymbol{C}\begin{bmatrix}\boldsymbol{B} & \boldsymbol{AB} & \cdots & \boldsymbol{A}^{q-1}\boldsymbol{B}\end{bmatrix}\begin{bmatrix}\boldsymbol{h}_1 \\ \vdots \\ \boldsymbol{h}_q\end{bmatrix} \tag{6}$$

A system is said to be output controllable if it is possible to construct inputs that will transfer any given initial output $\boldsymbol{y}(t_-)$ to any final output until the final time $t = t_+$. In a similar manner to state controllability, the necessary and sufficient condition for output controllability is that

$$\boldsymbol{N} \triangleq \boldsymbol{C}\begin{bmatrix}\boldsymbol{B} & \boldsymbol{AB} & \cdots & \boldsymbol{A}^{q-1}\boldsymbol{B}\end{bmatrix} = \boldsymbol{CV} \in \Re^{m\times qr} \tag{7}$$

has full rank m [9]. The matrix $\boldsymbol{N}$ is product of the matrices $\boldsymbol{C}$ and $\boldsymbol{V}$. Thus, if the system is state controllable, the necessary and sufficient condition for output controllability is that the matrix $\boldsymbol{C}$ has full rank.

Equations (6) and (7) reveal that the set of the output-controllable $\boldsymbol{y}$ steered by the input $\boldsymbol{u}$ of (3) is equivalent to the range space of the matrix $\boldsymbol{N}$. Thus, the set of the output-controllable $\boldsymbol{y}$, which is realizable by the input $\boldsymbol{u}$ normalized as $\boldsymbol{h}^T\boldsymbol{h} \leq 1$, forms an ellipsoid in the m-dimensional output space. The shape and size of the ellipsoid reflect the characteristic of the output controllability, which can be found by the singular value decomposition of the matrix $\boldsymbol{N}$.

Let the singular value decomposition of the matrix $\boldsymbol{N}$, which has full rank m, be described as

$$\boldsymbol{N} = \boldsymbol{U}_N\boldsymbol{\Sigma}_N\boldsymbol{V}_N^T = \sum_{i=1}^{m}\sigma_{Ni}\boldsymbol{u}_{Ni}\boldsymbol{v}_{Ni}^T \tag{8}$$

$$\boldsymbol{\Sigma}_N = \begin{bmatrix}\ \mathrm{diag}(\sigma_{N1}, \sigma_{N2}, \cdots, \sigma_{Nm}) & \boldsymbol{0}\ \end{bmatrix} \tag{9}$$

where $\sigma_{N1} \geq \sigma_{N2} \geq \ldots \geq \sigma_{Nm} > 0$ are the singular values, $\boldsymbol{U}_N$ and $\boldsymbol{V}_N$ are orthogonal matrices, the ith column vectors of which are $\boldsymbol{u}_{Ni}$ and $\boldsymbol{v}_{Ni}$, respectively, and $\boldsymbol{0}$ is a zero matrix. Thus, the set of output-controllable $\boldsymbol{y}$ can be described as an m-dimensional ellipsoid having principal axes $\sigma_{N1}\boldsymbol{u}_{N1}$, $\sigma_{N2}\boldsymbol{u}_{N2}$, …, $\sigma_{Nm}\boldsymbol{u}_{Nm}$ (referred to as the Output Controllability Ellipsoid: OCE), where $\boldsymbol{u}_{Ni}$ is the unit vector indicating the principal axis and σ_{Ni} is its radius. The magnitudes of the singular values represent the strengths of the effects of input on output [4], [6]. Therefore, the effect of input on output is relatively strong in the direction indicated by $\boldsymbol{u}_{Ni}$, which has a larger singular value σ_{Ni}.

There are the other indexes based on the controllability Gramian [11]. However, the derivation of the Gramians requires that the system matrix $\boldsymbol{A}$ is stable. A robotic arm generally has an unstable system matrix $\boldsymbol{A}$, as shown later herein. Thus, it is difficult to apply a Gramian-based evaluation to a robotic arm. In contrast, the evaluation based on an output controllability matrix is independent of the system stability. Therefore, it is possible to apply this evaluation to a robotic arm.

III. Performance Evaluation of Robotic Arm

A. State Equation of Robotic Arm

The equation of motion of a n degree-of-freedom robotic arm can be described as a time-variant non-linear system, such as

$$\boldsymbol{M}(\boldsymbol{\theta})\ddot{\boldsymbol{\theta}} + \boldsymbol{h}(\boldsymbol{\theta}, \dot{\boldsymbol{\theta}}) + \boldsymbol{g}(\boldsymbol{\theta}) = \boldsymbol{\tau} \tag{10}$$

where $\boldsymbol{\theta} \in \Re^n$ is the joint position, $\boldsymbol{\tau} \in \Re^n$ is the applied joint driving force, $\boldsymbol{M}(\boldsymbol{\theta}) \in \Re^{n\times n}$ is the inertia matrix, $\boldsymbol{h}(\boldsymbol{\theta},\ \dot{\boldsymbol{\theta}}) \in \Re^n$ is the centrifugal force and the Coriolis force, and $\boldsymbol{g}(\boldsymbol{\theta}) \in \Re^n$ is the gravitational force acting on the robotic arm.

Assuming that the position and orientation of the end-effector is described as $\boldsymbol{p} \in \Re^m$, the kinematic relation between $\boldsymbol{\theta}$ and $\boldsymbol{p}$ can be described as a non-linear function such as

$$\boldsymbol{p} = \boldsymbol{f}(\boldsymbol{\theta}) \tag{11}$$

To apply the linear systems theory discussed in section II to the robotic arm, we need to derive the linearized model of the robotic arm. Linearizing (10) and (11) with respect to the equilibrium points $\boldsymbol{\theta} = \boldsymbol{\theta}_e$, $\boldsymbol{\tau} = \boldsymbol{\tau}_e$, and $\boldsymbol{p} = \boldsymbol{p}_e$, which satisfy $\ddot{\boldsymbol{\theta}} = \dot{\boldsymbol{\theta}} = \boldsymbol{0}$, yields the linear time-invariant state equation and the output equation with n inputs, m outputs, and $2n$ state variables, as follows:

$$\frac{d}{dt}\begin{bmatrix}\delta\boldsymbol{\theta}(t) \\ \delta\dot{\boldsymbol{\theta}}(t)\end{bmatrix} = \boldsymbol{A}\begin{bmatrix}\delta\boldsymbol{\theta}(t) \\ \delta\dot{\boldsymbol{\theta}}(t)\end{bmatrix} + \boldsymbol{B}\delta\boldsymbol{\tau}(t) \tag{12}$$

$$\delta\boldsymbol{p}(t) = \boldsymbol{C}\begin{bmatrix}\delta\boldsymbol{\theta}(t) \\ \delta\dot{\boldsymbol{\theta}}(t)\end{bmatrix} \tag{13}$$

where

$$\boldsymbol{A} = \begin{bmatrix}\boldsymbol{0} & \boldsymbol{I}_n \\ -\boldsymbol{M}^{-1}\boldsymbol{G} & \boldsymbol{0}\end{bmatrix}_{\theta=\theta_e},\quad \boldsymbol{B} = \begin{bmatrix}\boldsymbol{0} \\ \boldsymbol{M}^{-1}\end{bmatrix}_{\theta=\theta_e} \qquad \boldsymbol{C} = \begin{bmatrix}\boldsymbol{J} & \boldsymbol{0}\end{bmatrix}_{\theta=\theta_e} \tag{14}$$

$\boldsymbol{I}_n$ is an $n\times n$ identity matrix, and $\boldsymbol{J}$ and $\boldsymbol{G}$ are the Jacobian matrices concerning the structure of the robotic arm and the gravitational force, respectively. Jacobians $\boldsymbol{J}$ and $\boldsymbol{G}$ are given by

$$\boldsymbol{J}(\boldsymbol{\theta}) = \frac{\partial\boldsymbol{f}}{\partial\boldsymbol{\theta}} \in \Re^{m\times n}, \qquad \boldsymbol{G}(\boldsymbol{\theta}) = \frac{\partial\boldsymbol{g}}{\partial\boldsymbol{\theta}} \in \Re^{n\times n} \tag{15}$$

where $\delta\boldsymbol{\theta}(t) = \boldsymbol{\theta}(t) - \boldsymbol{\theta_e}$, $\delta\dot{\boldsymbol{\theta}}(t) = \dot{\boldsymbol{\theta}}(t) - \dot{\boldsymbol{\theta}}_e$, $\delta\boldsymbol{\tau}(t) = \boldsymbol{\tau}(t) - \boldsymbol{\tau}_e$, and $\delta\boldsymbol{p}(t) = \boldsymbol{p}(t) - \boldsymbol{p}_e$.

B. Output Controllability of the Robotic Arm

The controllability matrix $\boldsymbol{V}$ and the output controllability matrix $\boldsymbol{N}$ of the robotic arm can be obtained by substituting the matrices $\boldsymbol{A}$, $\boldsymbol{B}$, and $\boldsymbol{C}$ of (14) into (5) and (7), respectively. This yields

$$\boldsymbol{V} = \begin{bmatrix} \boldsymbol{0} & \boldsymbol{M}^{-1} & \cdots & (-\boldsymbol{M}^{-1}\boldsymbol{G})^{n-1}\boldsymbol{M}^{-1} \\ \boldsymbol{M}^{-1} & \boldsymbol{0} & \cdots & \boldsymbol{0} \end{bmatrix} \quad (16)$$

$$\boldsymbol{N} = \boldsymbol{J}\Big[\ \boldsymbol{0} \quad \boldsymbol{M}^{-1} \quad \boldsymbol{0} \quad (-\boldsymbol{M}^{-1}\boldsymbol{G})\boldsymbol{M}^{-1}\cdots \cdots(-\boldsymbol{M}^{-1}\boldsymbol{G})^{n-1}\boldsymbol{M}^{-1}\Big] \quad (17)$$

If the controllability matrix $\boldsymbol{V} \in \Re^{2n\times 2n^2}$ has full rank, then the robotic arm is state controllable, and the joint position can be arbitrary steered by the joint driving force. Since the inertia matrix $\boldsymbol{M}$ has generally full rank, (16) indicates that the controllability matrix $\boldsymbol{V}$ always has full rank. Therefore, a robotic arm is necessarily state controllable.

If the output controllability matrix $\boldsymbol{N} \in \Re^{m\times n^2}$ has full rank, then the robotic arm is output controllable, and the position and orientation of the end-effector can be arbitrary steered by the joint driving force. Since a robotic arm is always state controllable, the necessary and sufficient condition for a robotic arm to be output controllable is that the structure Jacobian $\boldsymbol{J}$ has full rank, as stated in Section II. Thus, a robotic arm maintains output controllability unless the configuration of a robotic arm is singular.

In the above discussion, we have assumed that there is no constraint imposed on the maximum joint driving forces and that the weights of the components related to the translational and rotational motion of the end-effector are the same. When these assumptions do not hold, normalization of input and/or output variables is needed [12].

C. Performance Evaluation based on Output Controllability Ellipsoid

The size and shape of the output controllability ellipsoid (OCE) indicate the characteristics of output controllability (Fig. 2). The major axis of the OCE can be obtained as $\sigma_{N1}\boldsymbol{u}_{N1}$, where σ_{N1} is the maximum singular value and $\boldsymbol{u}_{N1}$ is its singular vector, as shown in (8). By steering the position and orientation of the end-effector in this direction, the effect of the joint driving force (input) on the position and orientation (output) of the end-effector is maximized. Therefore, we can minimize the joint driving force by steering its end-effector in this direction from the equilibrium point. This means that the mechanical efficiency is the highest. (In robotics, the mechanical efficiency is described as the manipulability [12].) Note that the control accuracy is the lowest in this direction. Since the robotic arm has high-sensitivity in this direction, even a small input error, such as noise, greatly affects the motion of the end-effector.

The minor axis of the OCE can be obtained as $\sigma_{Nm}\boldsymbol{u}_{Nm}$ when the matrix $\boldsymbol{N}$ has full rank m. The effect of the joint driving force (input) on the position and orientation (output) of the end-effector is the lowest in this direction. The maximum joint driving force is needed in order to steer the end-effector in this direction from the equilibrium point. This means that the mechanical efficiency is the lowest. However, the control accuracy is the highest since the robotic arm has low sensitivity in this direction.

Using the OCE makes it possible to evaluate the performance of a robotic arm with respect to efficiency and accuracy. In general, high efficiency and high accuracy are desired for a robotic arm. Since the major axis indicates the direction of high efficiency and low accuracy and on the other hand the minor axis indicates the direction of low efficiency and high accuracy, the two performances cannot be satisfied simultaneously. For the performance evaluation based on the OCE, we are required to take the above characteristics into consideration.

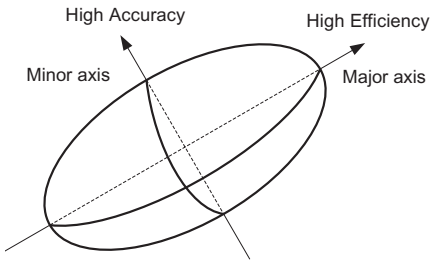

Fig. 2. Output controllability ellipsoid

D. Performance Measure

From (17), the output controllability matrix $\boldsymbol{N}$ consists of the gravitational Jacobian matrix $\boldsymbol{G}$, the structure Jacobian matrix $\boldsymbol{J}$, and the inertia matrix $\boldsymbol{M}$. Thus, the output controllability depends not only on the configuration and dynamic parameters of a robotic arm, but also on the gravity loads acting on the robotic arm.

For the quantitative evaluation of its performance, the performance measure can be described as follows.

1) Volume Measure ν [6]:

$$\nu(\boldsymbol{N}) = (\det(\boldsymbol{N}\boldsymbol{N}^T))^{1/2} = \sigma_{N1}\sigma_{N2}\cdots\sigma_{Nm} \quad (18)$$

The volume measure ν, which shows the volume of the OCE, indicates the degree of the effect of the joint driving force (input) on the position and orientation (output) of the end-effector. Therefore, if ν becomes larger, then the mechanical efficiency becomes higher, while if ν becomes smaller, the control accuracy becomes higher.

2) Condition Number Measure μ [4]:

$$\mu(\boldsymbol{N}) = \sigma_{Nm}/\sigma_{N1} \leq 1.0 \quad (19)$$

The condition number measure μ is the ratio of the maximum and minimum radii of the OCE, which indicates the isotropic measure of the OCE. The closer this index is to unity, the closer the shape of the OCE is to a sphere and the better the balance between the control accuracy and the mechanical efficiency. In addition, the closer this index is to zero, the

more the OCE is squeezed along the minor axis, and the worse the balance between the control accuracy and the mechanical efficiency. Therefore, the performance is notably different, depending on the steering direction of the end-effector.

E. Difference between Output Controllability and Dynamic Manipulability

The dynamic manipulability gives a measure of the ability of performing end-effector accelerations along each task space direction for a given set of joint driving forces [12]. Assuming the robotic arm is at rest, substituting (10) into the equation obtained by differentiating (11) with respect to time yields the relation between the joint driving forces (input) and the end-effector accelerations (output), as follows:

$$\ddot{\boldsymbol{p}} = \boldsymbol{J}\boldsymbol{M}^{-1}\widetilde{\boldsymbol{\tau}} \tag{20}$$

where $\widetilde{\boldsymbol{\tau}} = \boldsymbol{\tau} - \boldsymbol{g}$. As shown by (20), the current outputs are determined only by the current joint driving forces, but also they are independent of past inputs. Thus, the dynamic manipulability is restricted to the measure of the instantaneous process between inputs and outputs in a robotic arm system.

On the other hand, in the case of the output controllability, the current outputs are affected by the joint driving forces and the gravitational loads that are applied to the robotic arm from the past to the present, as mentioned before. The current outputs are dependent on current and past inputs. Thus, the output controllability can be viewed as a measure of the dynamic process between inputs and outputs in a robotic arm system. The evaluation that takes into account the dynamic process and the effects of gravity for a finite time interval is desirable with respect to motion control and motion planning.

We deal with a particular robotic arm in a zero gravity field (ex., the space shuttle robotic arm). Since the gravity is zero, substituting $\boldsymbol{G} = \boldsymbol{0}$ into (17) yields

$$\boldsymbol{N} = \begin{bmatrix} \boldsymbol{0} & \boldsymbol{J}\boldsymbol{M}^{-1} & \boldsymbol{0} & \cdots & \boldsymbol{0} \end{bmatrix}$$

The singular values and the singular vectors of $\boldsymbol{N}$ coincide with those of $\boldsymbol{J}\boldsymbol{M}^{-1}$ in (20). When the state variable is independent of the effect of gravity, the concept of the output controllability coincides with that of the dynamic manipulability.

IV. Simulation

In order to verify the performance measure based on the output controllability, we conduct example simulations using the two degree-of-freedom robotic arm in the vertical plane shown in Fig. 3. We define the end-effector position as the output variable. Gravity is exerted in the $-y$ direction. Let m_i be the mass of the ith link, and let l_i be the length of the ith link. In addition, let l_{gi} be the length to the center of mass of the ith link, and let I_i be the moment of inertia about the center of mass of the ith link.

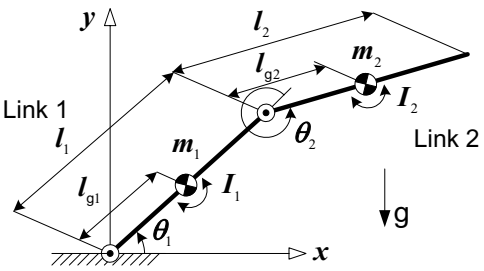

Fig. 3. Two degree-of-freedom robotic arm ($l_1 = l_2 = 1\text{m}$, $l_{g1} = l_{g2} = 0.5\text{m}$, $m_1 = 30\text{kg}$, $m_2 = 15\text{kg}$, $I_1 = 30/12\text{kg}\cdot\text{m}^2$, $I_2 = 15/12\text{kg}\cdot\text{m}^2$)

A. Effect of Gravity on Output Controllability

This section verifies the effect of gravity on the output controllability. We first observe the difference between the output controllability under gravity and that under zero gravity. The OCE can be obtained as Fig. 4 when neglecting the gravity effect. Figs. 4(a) and (b) show the OCE obtained by setting $\theta_2 = 30$ and 60 deg, respectively, and varying θ_1 from -90 to 90 deg, where the figure of the OCE is enlarged ten times. Figs. 4(c) and (d) show the volume measure ν and the condition number measure μ, respectively, for each value of θ_2. In this case, the output controllability depends only on the value of θ_2. If θ_2 is constant, both ν and μ remain constant. Therefore, even if the configuration is changed as shown in Figs. 4(a) or (b), the size and isotropy of the OCE never change.

On the other hand, when taking gravity into consideration, the OCE is given as Fig. 5. Figs. 5(a) and (b) show the OCE of the same configuration as used in Figs. 4(a) and (b). Figs. 5(c) and (d) show the volume measure ν and the condition number measure μ, respectively. According to the change of the gravitational load by the variation of configuration, both of the measures are also changed. This yields a change in the size and isotropy of the OCE. In addition, as shown in Figs. 4(c) and 5(c), the size of the OCE under gravity is larger than that of the OCE under zero gravity. Therefore, gravity causes not only high efficiency but also low control performance in a robotic arm. In addition, the balance between the efficiency and the accuracy depends on the gravitational load. As shown above, gravity clearly has a large effect on the output controllability. Thus, it is necessary to consider the effects of gravity.

Next, we verify the configurations that have the minimum and maximum effect of gravity. The effect of gravity on the output controllability depends only on the gravitational Jacobian $\boldsymbol{G}$, as shown in (17). Hence, the magnitude of the eigenvalue of the gravitational Jacobian indicates the effect of gravity on the output controllability. Here, we obtain the determinant of $\boldsymbol{G}$ as the product of the eigenvalues.

The gravitational load of the two degree-of-freedom robotic arm can be obtained as

$$\boldsymbol{g}(\boldsymbol{\theta}) = \begin{bmatrix} (m_1 l_{g1} + m_2 l_1) g c_1 + m_2 l_{g2} g c_{12} \\ m_2 l_{g2} g c_{12} \end{bmatrix} \tag{21}$$

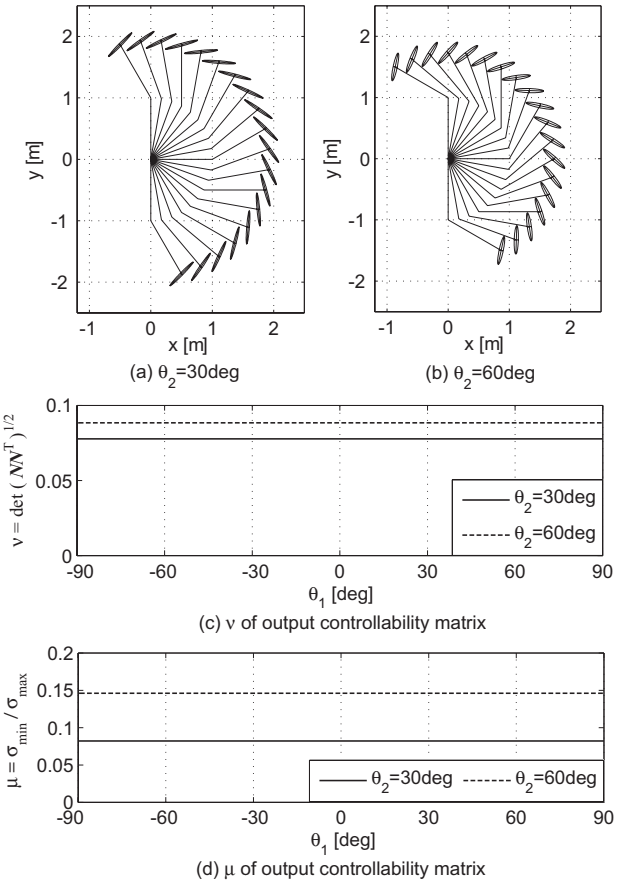

Fig. 4. Output controllability ellipsoid without gravity

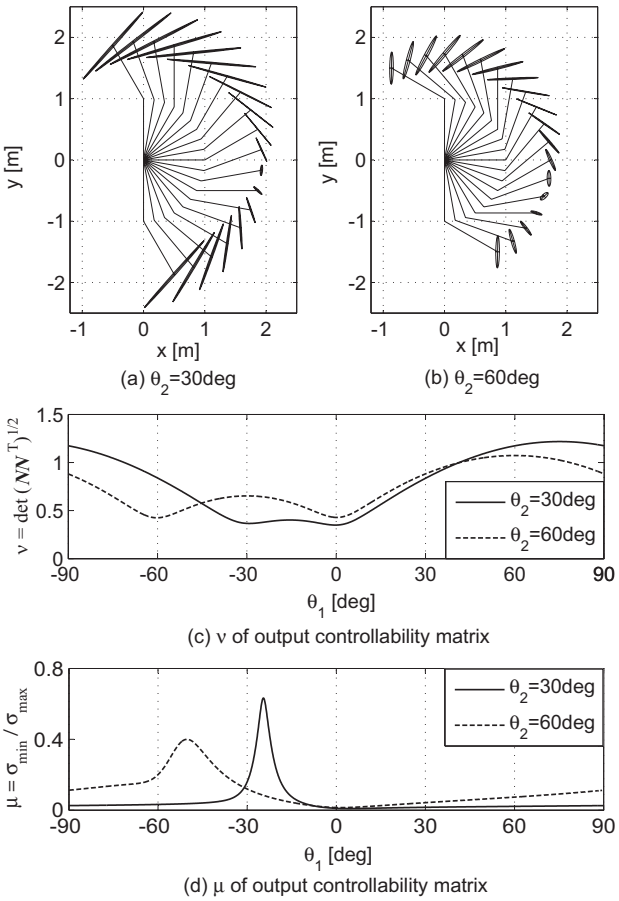

Fig. 5. Output controllability ellipsoid with gravity

where $c_i = \cos\theta_i$, $s_i = \sin\theta_i$, $c_{12} = \cos(\theta_1 + \theta_2)$, and $s_{12} = \sin(\theta_1 + \theta_2)$. Equation (15) yields the gravitational Jacobian such as

$$\boldsymbol{G} = \frac{\partial \boldsymbol{g}}{\partial \boldsymbol{\theta}} = \begin{bmatrix} \alpha + \beta & \beta \\ \beta & \beta \end{bmatrix} \tag{22}$$

where $\alpha = (m_1 l_{g1} + m_2 l_1) g s_1$ and $\beta = m_2 l_{g2} g s_{12}$. Thus, the determinant of $\boldsymbol{G}$ can be obtained as

$$\det\boldsymbol{G} = m_2 l_{g2} (m_1 l_{g1} + m_2 l_1) g^2 s_1 s_{12} \tag{23}$$

When $\det\boldsymbol{G} = 0$, the effect of gravity is minimum. The following three cases are obtained from (23), which are (i) $s_1 = 0$, (ii) $s_{12} = 0$, and (iii) $l_{g2} = 0$, where we take $m_1 > 0$ and $m_2 > 0$ into consideration. Figs. 6(a) and (b) show the configuration examples given as cases (i) and (ii), respectively. In case (i), only link 1 is horizontal, and in case (ii) only link 2 is horizontal. The configuration satisfying case (iii) has the center of gravity of link 2 on the second joint. In particular, if $s_1 = s_{12} = 0$, at which links 1 and 2 are horizontal, as shown in Figs. 6(c) and (d), the gravitational Jacobian becomes $\boldsymbol{G} = \boldsymbol{0}$, and so there is no effect of gravity on the state variables.

On the other hand, at the point where the effect of gravity is maximum, $|\det\boldsymbol{G}|$ achieves the maximum value. Here, $\det\boldsymbol{G}$ is proportional to $s_1 s_{12}$, and so $|\det\boldsymbol{G}|$ achieves the maximum value when $|s_1 s_{12}| = 1$, which indicates that links 1 and 2 are in the vertical direction, as shown in Figs. 7(a) and (b). The joint angle θ_1 exerting the maximum effect of gravity for a given θ_2 can be obtained by deriving the extremum of $\det\boldsymbol{G}$. The joint angles θ_1 and θ_2 satisfying the above conditions form an isosceles triangle, the three apexes of which are the first joint, the second joint, and the point at the intersection between the y axis and the half line from the second joint to the end-effector. If links 1 and 2 have the same length, then the end-effector is located on the y axis, as shown in Fig. 7(c).

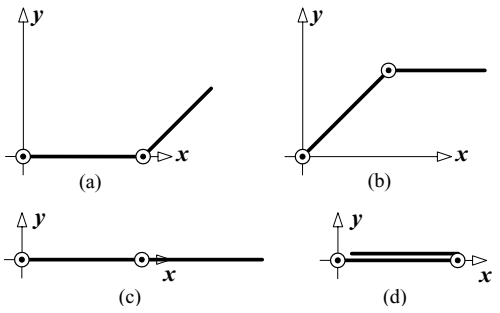

Fig. 6. Configurations of the robotic arm that have the minimum effect of gravity

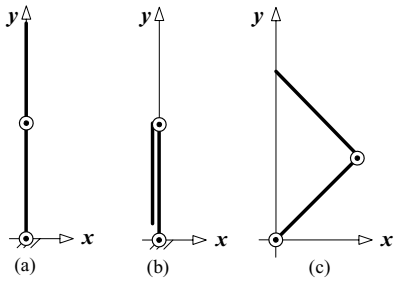

Fig. 7. Configurations of the robotic arm that have the maximum effect of gravity

The above discussion is verified using the results shown in Fig. 5(c). The volume measure ν of $\theta_2 = 30$ deg becomes the minimum when $\theta_1 = 0$ and -30 deg. The robotic arms in which $\theta_1 = 0$ deg and $\theta_1 = -30$ deg, respectively, have horizontal links 1 and 2. Thus, the effect of gravity becomes the minimum in these configurations and the control accuracy then becomes the highest. The same is true for the simulation results of $\theta_2 = 60$ deg.

On the other hand, the volume measure ν of $\theta_2 = 30$ and 60 deg becomes the maximum when $\theta_1 = 75$ and 60 deg, respectively. The end-effectors of these configurations are located on the y axis. Thus, the effect of gravity becomes the maximum. The mechanical efficiency then becomes the maximum, but the control accuracy becomes the lowest.

In this section, the performance of a robotic arm has been shown to depend deeply on the effect of gravity. In addition, configurations that have lower effects of gravity can achieve the higher control accuracy. In contrast, configurations that have higher effects of gravity can achieve higher mechanical efficiency.

B. Application to Trajectory Planning

The desired trajectory for a robotic arm is set on a workspace such that the motion of the end-effector is not adversely affected by small errors from a nominal joint driving torque. We first discuss the difference in performance of the robotic arm between the optimal trajectory obtained by taking the effect of gravity into consideration and that obtained by without considering the effect of gravity.

Fig. 8 shows the OCE for the cases with and without gravity on the same scale. From this figure, even though the end-effector is located at the equivalent position, $\boldsymbol{p}_0 = (-1.5,\ 0.75)$ m, the volumes, shapes, and orientations of the OCEs are totally different. Thus, it is not necessarily the case that the minimum sensitive direction with gravity coincides with that without gravity.

Assuming that the end-effector moves the same distance in a straight line from $\boldsymbol{p}_0$ along the major axis of each OCE, we compare the position errors of the end-effector at each final point. The nominal joint torque for each trajectory is obtained from (10) and (11) in advance. The input torque is set as the sum of its nominal joint torque and the Gaussian white noise. Applying the input torque to the feedforward controller, we obtain the final position of the end-effector.

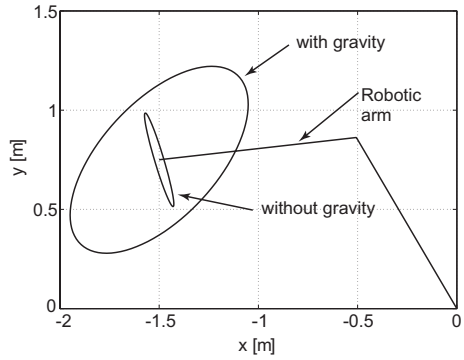

Fig. 8. Output controllability ellipsoid for the cases with and without gravity

This simulation is repeated 100 times. We let the moving distance be 0.2 m, the total motion time be 1.5 s, and the variance of the Gaussian white noise be $(25,\ 25)$ $\mathrm{N}^2\mathrm{m}^2$.

Figs. 9(a) and (b) show the respective probability distributions of the final position of the end-effector for trajectories with and without taking gravity into account. The ellipse in each figure shows the two-σ error ellipse centered at the average final position of the end-effector, where σ indicates the standard deviation. The distribution of the final position for the trajectory planned considering the effect of gravity (Fig. 9(a)) is smaller than that planned without considering the effect of gravity (Fig. 9(b)). This means that the robotic arm can be controlled more precisely by taking gravity into consideration.

This difference in control accuracy arises from the difference in the direction of the principal axis of the OCE in Fig. 8. Since the end-effector is insensitive in the direction of the minor axis of the OCE, the end-effector is least affected by input errors in this direction. Therefore, in order to control the robotic arm precisely, the trajectory should be set such that the normal corresponds with the minor axis and the tangent corresponds with the major axis to the greatest extent possible. In addition, the gravity should be taken into account explicitly.

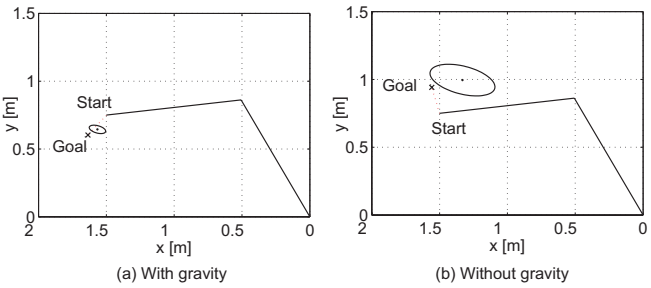

Fig. 9. Probability distribution of the final position of the end-effector for trajectories with and without taking gravity into account

The two degree-of-freedom robotic arm has two configurations that can trace the same position trajectory, as shown in Fig. 10. However, such configurations have OCEs of different

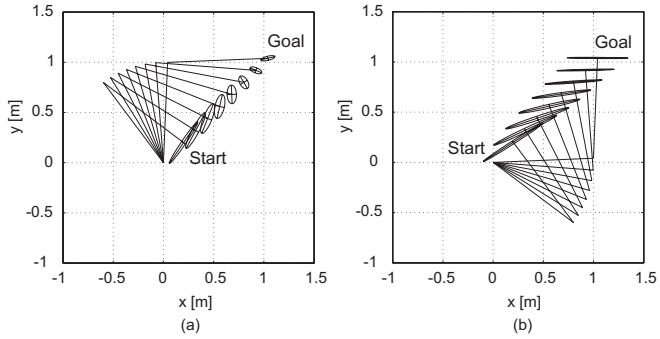

Fig. 10. Trajectory planning for two different configurations

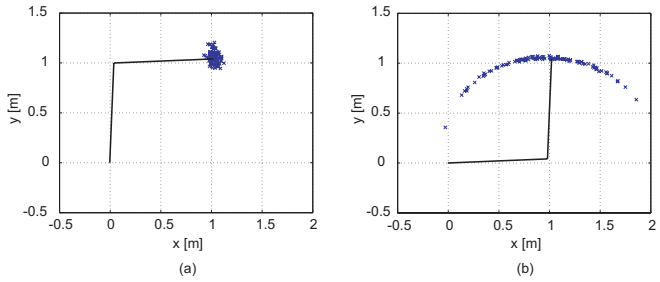

Fig. 11. Position errors at final position of end-effector for two different configurations

volumes, shapes, and orientations. We discuss the effect of the difference of the configuration on the trajectory planning.

The second simulation is conducted under the same condition as that of the simulation in Fig. 9. We apply the feedforward controller to the robotic arm and obtain the final positions of the end-effector by repeating this procedure 100 times. The final positions of the end-effector are denoted by $\times$ in Figs. 11(a) and (b) for each trajectory, which corresponds to the case shown in Figs. 10(a) and (b), respectively. The final positions in Fig. 11(a) converge around the desired goal point, while the final positions in Fig. 11(b) are widely dispersed. Fig. 11(a) gives a more accurate manipulation than (b), because, as shown in Fig. 10, compared to the configuration of (b), the configuration of (a) has a lower sensitivity in the perpendicular direction of the given trajectory.

Therefore, since the different configurations have the totally different control accuracies, even if these can trace the same trajectory, it is important to select the optimal configuration according to the task.

V. Conclusion

The present paper proposed an evaluation of the manipulation performances with respect to the control accuracy and the mechanical efficiency of a robotic arm, taking gravity into consideration.

The following are the findings of the present paper: (1) The output controllability ellipsoid expresses the set of the variation of the position and the orientation of the end-effector from its equilibrium point when the joint driving forces are slightly perturbed. (2) A trade-off relationship exists between the control accuracy and the mechanical efficiency. (3) The output controllability includes the gravitational effect. (4) The proposed measure is obtained by considering the dynamic process between inputs and outputs in a robotic arm system.

The simulation results revealed the following: (1) Gravity has a significant effect on the manipulation performance for the mechanical efficiency and the control accuracy. (2) The robotic arm has particular configurations that can achieve the best manipulation performance for each performance measure. (3) The proposed measures generate an improvement in the control accuracy by planning a trajectory in which the normal direction corresponds to the minor axis of the OCE.

The proposed measures, which are based on the output controllability of the linearized dynamic robot model, are valid for various types of practical robots, to which the linear system theory can be applied. In the future, the applicability of the measure shall be extended to robotic systems that have complicated constraints, such as friction or non-holonomic constraints. We will also consider task-oriented manipulation explicitly, taking the gravitational effect into consideration.

References

[1] H. Asada,"A geometrical representation of menipulator dynamics and its application to arm design," Trans. of ASME, J. Dynamics Systems, Measuremet and Control, vol.105, no.3, pp.131-135, 1983.

[2] P. Chiacchio, S. Chiaverini, L. Sciavicco and B. Siciliano, "Influence of Gravity on the Manipulability Ellipsoid for Robot Arms," Trans. of ASME, J. Dynamics Systems, Measuremet and Control, pp.723-727, December 1992.

[3] S. L. Chiu, "Task Compatibility of Manipulator Postures," The Int. J. of Robotics Research, vol.7, no.5, pp.13-21, 1988.

[4] B. Friedland, "Controllability Index based on Conditioning Number," Trans. of ASME, J. Dynamics Systems, Measuremet and Control, pp.444-445, December 1975.

[5] T. J. Graettinger and B. H. Krogh, "The Acceleration Radius: A Global Performance Measure for Robotic Manipulators," IEEE J.of Robotics and Automation, vol.4, no.1, pp.60-69, 1988.

[6] C. D. Johnson, "Optimization of a Certain Quality of Complete Controllability and Observability for Linear Dynamical Systems," Trans. of ASME, J. Basic Engineering, pp.228-238, June 1969.

[7] T. Kailath, Linear Systems, Prentice-Hall 1980.

[8] C. A. Klein and B. E. Blaho, "Dexterity Measures for the Design and Control of Kinematically Redundant Manipulators ," The Int. J. of Robotics Research, vol.6, no.2, pp.72-83, 1987.

[9] E. Kreindler and P. E. Sarachik, "On the Concepts of Controllability and Observability of Linear Systems," IEEE Trans. on Automatic Control, vol.9, no.2, pp.129-136, 1964.

[10] O. Ma and J. Angeles, "Optimal Design of Manipulators under Dynamic Isotropy Conditions," Proc. IEEE Int. Conf. on Robotics and Automation, pp.2424-2429, 1993.

[11] B. C. Moore, "Principal Component Analysis in Linear Systems: Controllability, Observability and Model Reduction," IEEE Trans. Automatic Control, vol.26, no.1, pp.17-32, 1981.

[12] T. Yoshikawa, Foundations of Robotics, MIT Press, 1990.